

Article

Sustainable Basalt Fibers vs. Traditional Glass Fibers: Comparative Study on Thermal Properties and Flow Behavior of Polyamide 66-Based Composites

Antonella Patti ¹, Stefano Acierno ², Luigi Nele ³, Lucia Graziosi ⁴ and Domenico Acierno ^{4,*}

¹ Department of Civil Engineering and Architecture (DICAr), University of Catania, Viale Andrea Doria 6, 95125 Catania, Italy

² Department of Engineering, University of Sannio, Piazza Roma 21, 82100 Benevento, Italy

³ Department of Chemical, Materials and Industrial Production Engineering, University of Naples Federico II, Piazzale Tecchio 80, 80125 Naples, Italy

⁴ Regional Center of Competence New Technologies for Productive Activities Scarl, Via Nuova Agnano 11, 80125 Naples, Italy

* Correspondence: acierno@crdctecnologie.it

Abstract: In this work, basalt fibers (BF) have been investigated as possible natural and sustainable replacements for the common synthetic mineral filler—glass fibers (GF)—used in polyamide 66 matrix (PA66). Composites have been prepared at two different fiber concentrations (15 and 25 wt.%, respectively) by melt blending. The developed systems have been mainly characterized by thermogravimetric analysis (TGA), differential scanning calorimetry (DSC), capillary rheology, and scanning electron microscopy (SEM). The kinetic parameters to thermal degradation through the Coats–Redfern method allowed us to attest a negligible effect of fiber type on thermal stability of the developed systems. Composites incorporating 15 wt.% of fiber content possessed the highest activation energy (≥ 230 kJ/mol). The introduction of BF and GF in PA 66 polymer, regardless of content, always led to an increase in crystallization and melting temperatures, and to a similar reduction in crystallinity degree and glass transition temperature. The shear viscosity of the basic polymer increased by the addition of fillers, particularly at low shear rate, with a pronounced effect in the case of basal fibers. A slightly higher shear thinning behavior of BF/PA66 with respect to GF/PA66 composites was confirmed by fitting the flow curves through the power law model. Finally, a worsening in fiber dispersion, by increasing the content in the matrix, and a weak compatibility between the two phases constituting the materials were highlighted through SEM micrographs.

Keywords: basalt fibers; glass fibers; polyamide 66; thermal properties; flow behavior; processing aspects



Citation: Patti, A.; Acierno, S.; Nele, L.; Graziosi, L.; Acierno, D. Sustainable Basalt Fibers vs. Traditional Glass Fibers: Comparative Study on Thermal Properties and Flow Behavior of Polyamide 66-Based Composites. *ChemEngineering* **2022**, *6*, 86. <https://doi.org/10.3390/chemengineering6060086>

Received: 30 August 2022

Accepted: 20 October 2022

Published: 4 November 2022

Publisher's Note: MDPI stays neutral with regard to jurisdictional claims in published maps and institutional affiliations.



Copyright: © 2022 by the authors. Licensee MDPI, Basel, Switzerland. This article is an open access article distributed under the terms and conditions of the Creative Commons Attribution (CC BY) license (<https://creativecommons.org/licenses/by/4.0/>).

1. Introduction

The most common materials, used as reinforcement, in polymer resins are: steel, asbestos (fibrous silicate mineral), aramid, and carbon [1]. Each of them possesses advantages and disadvantages. For example: steel is endowed with an exceptional mechanical strength but also an elevated density. Steel fibers possess a density (7.85 g/cm³) about three times higher than glass fibers (2.46 g/cm³), and four times higher than carbon fibers (1.76 g/cm³) [2]. Carbon fibers are one of the most expensive fibers, followed by aramid fibers [3]. The asbestos fibers have good characteristics, as strength, durability, flexibility, and resistance to corrosion, heat, and fire, but are considered harmful given the carcinogenic response in the human body [4].

Recently, basalt has been proposed as the “twenty-first century non-polluting green material” [5]. Basalt fibers possess similar performance to glass fibers, and are cheaper compared to carbon fibers [6]. Although more persistent in biological structures, basalt

fibers have displayed a lower acute toxicity and less fibrogenic and carcinogenic activity compared to chrysotile asbestos [7].

Basalt is an aphanitic igneous extrusive (volcanic) rock formed by the rapid cooling of basaltic lava, equivalent to gabbro-norite magma [8]. Its chemical composition is made prevalently from silicon dioxide (SiO_2 , <51.5 wt.%), aluminum oxide (Al_2O_3 , <19.0 wt.%), magnesium oxide (MgO , <10.5 wt.%), iron oxide ($\text{FeO} + \text{Fe}_2\text{O}_3$, <12.0 wt.%), sodium and potassium oxide ($\text{K}_2\text{O} + \text{Na}_2\text{O}$, <6 wt.%), and other remaining species, including titanium oxide (TiO_2), Chromium(III) oxide (Cr_2O_3), manganese oxide (MnO) [9].

Basalt is hard and dense, directly suitable for fiber manufacturing. Basalt fibers (BF) are produced in a single step process of melting and extruding the raw material at temperatures of 1400–1500 °C and drawing it to form fibers. Contrary to glass fiber (GF) production, no additives (chemicals, solvents, pigments, or hazard materials) are applied during the manufacturing process of basalt fibers [10].

Due to the growing attention of governments and environmental agencies towards the increasing amount of waste products abandoned in the landfill and polluting disposal operations, several solutions are proposed to recover plastic waste [11] and shift the production towards more ecofriendly solutions [12]. The common procedures to reclaim fibers from reinforced composites are mechanical methods, pyrolysis, oxidation in fluidized beds and chemical recycling [13]. However, thermal incineration remains the most preferred among them: at elevated temperatures (450–600 °C), the polymer matrix is burned off, leaving the residual char and the fibers [14]. Following incineration, the basalt powder can be employed once again, as a reinforcement, in new composite formulations [13]. The recycling of basalt fiber can be done in much better environmentally friendly ways than glass fibers [15]. In fact, during the incineration of discarded glass fiber-based composites, a great amount of black smoke and bad odors are generated. Often glass fibers are melted and create damage to the implants. Moreover, the decomposition of synthetic fibers is not easy and causes a strong environmental load on the reclamation process [5].

For these reasons, basalt fibers are also considered green, sustainable, natural materials that do not create environmental problems, pose pollution issues, and produce less risks for the health and safety of humans [16].

Basalt-based composites have been proposed for application in transportation infrastructure [17], in civil engineering [18], in marine structures [19], in automotive [13], and more recently in armors for ballistic protection [20], in wind turbines [21], in clean energy and power grids [16], in thermal insulation [22], and in offshore industry [23].

However, until now, the effect of basalt fibers to improve the mechanical and thermal properties of polymer matrices has not been fully investigated [24].

Polyamide (PA) is the first synthetic thermoplastic semicrystalline polymer, well-known by the name of Nylon. Its chemical structure is made up of an amide group ($-\text{CONH}-$) as a regular repeating portion of the macromolecular chain. The excellent mechanical strength, the temperature-resistant properties, the high resistance to friction, scratching and solvents, and the noise absorption performances allow the use of polyamide in applications to replace metals, and to satisfy the demand of engineering plastics in electronic, electrical and automobile industries, in household appliances, and sporting goods [25].

Depending upon the monomer used during synthesis, different types of polyamides (PA 6, PA 66, PA 11, PA 12, PA 6,12) can be realized. PA 66 is an important member of the PA family, often applied in automobiles, textiles, and decoration sectors, characterized by a high stiffness and mechanical strength over a wide temperature range [26], and a short-term thermal resistance linked to the high melting point [27]. The repeating unit of PA 66 is constituted of two monomers: the first is the adipic acid, the second is hexamethylene diamine. Each monomer contains six carbon atoms and carries amino and carboxylic acid as functional groups [28]. Mineral fillers or several fibers are considered the common reinforcing agents in composite materials since they lead to an improvement of the mechanical properties of polymer matrix, and at the same time to a reduction in the cost. The typical

mineral filler introduced in PA 66 resin is glass fiber: the resulting PA66/GF composites are mostly applied for the manufacture of high strength parts, especially in the automotive and industries provision of sports and leisure materials [27].

The non-isothermal crystallization of the polyamide 66 matrix and its composites with glass fiber has been investigated by DSC in the study of Makhlouf et al. [27]. The crystallization temperature of PA 66/GF composites was found to be up to 7 °C higher than that of the neat matrix.

The thermal behavior of nylon-66 and GF/nylon-66 at 30 wt.% of fiber content was examined by thermogravimetric analysis (TGA) and its derived thermogram (DTA). This characterization has been considered useful for proper understanding of the material processing and fabrication. Activation energy for the polymer degradation, calculated through two different methods (Murray–White and Coats–Redfern) was higher for GF/PA 66 composites compared with unfilled matrix. This finding was intended as a higher thermal stability due to the fiber introduction in neat PA66 polymer [29].

In this framework, this study aimed to attest the potential applicability of basal fibers to replace the most commonly used glass fibers in polyamide 66 resin. Attention was focused to identify the initial decomposition temperature, the glass transition temperature, the melting and crystallization point, and the shear viscosity. Final outcomes provided useful information on material processing of GF/PA66 and BF/PA66 composites. Usually, the main phases of material process consist of: melting of solid particles, molding into defined shape, and solidification of final product. The knowledge of the thermal stability indicates the limit at which the material can be considered intact (not decomposed) under the influence of temperature. The glass transition indicates the starting point at which the material could be considered workable. The crystallization point denotes the temperature at which, starting from the melted state and then cooling, the polymer macromolecules arrange themselves to form ordered structures. This phenomenon, linked to the cooling degree of the sample during the material shaping, impacts on the processing time and cost. The melting temperature, i.e., the condition at which the ordered polymer crystalline structure is broken through the supplying of heat, controls the energy requirement during the manufacturing process, more than cooling and solidification. The melt resistance affects the resistance to the screw rotation and drive power. The higher the melt resistance the more difficult the material flows within the channel.

2. Materials and Methods

2.1. Materials

The matrix used in this study was a polyamide 66 resin (cod. DURETHANE A30SFN31000000, density = 1169 kg/m³ ISO1183) supplied by Lanxess (Cologne, Germany). The chopped E-glass fibers (cod. ThermoFlow CS EC 13672, 4 mm in average length and 13 µm in average diameter) were supplied by Johns Manville (Denver, CO, USA). The chopped basalt fibers (cod. BCS17-6.4-KV16, 6.4 mm in average length and 17 µm in average diameter) were provided by Basaltex (Wevelgem, Belgium).

2.2. Composites Preparation

GF/PA-66 and BF/PA 66 composites were prepared by melt compounding in an intermeshing twin screw extruder PolyLab Haake by Thermo Fisher Scientific (Waltham, MA, USA) (screw diameter of 24 mm, L/D equal to 40) at a screw speed of 60 rpm. The following profile of temperature was set from hopper to die: 250, 260, 270, 270, 270, 290, 290, 270, 270 °C. The extruded outgoing composite filament was suddenly cooled in air, by passing through a series of rollers, and finally pelletized. Formulations containing 15 and 25% by wt. of fibers were prepared. The maximum value of 25 wt.% in fibers content was considered a design choice to avoid an excessive increase in the sample weight (glass fibers density is more than double that of composites) and complications during the extrusion phase (due to a potentially excessive increase in the melt viscosity).

It is well known that polyamide tends to absorb moisture. A hydrolysis mechanism takes place, and the PA 66 polymer chains are broken by reducing the properties of PA 66-based composites [30]. For this reason, before the compounding and sample testing, each material was dried in an oven for 4 h at temperature of 80 °C.

2.3. Characterization Techniques

2.3.1. Thermogravimetric Analysis (TGA)

Thermogravimetric measurements were performed in a Q500 TGA, produced by TA Instruments, (New Castle, DE, USA). A piece of material (weight around 10–13 mg) was heated from room temperature to 700 °C at a rate of 10 °C/min in an inert atmosphere of nitrogen. During the measurement, sample weight as a function of temperature was recorded. On this plot, the initial decomposition temperature was considered the temperature in correspondence of 5% in wt. of mass loss ($T_{dec5\%}$). The temperature at which the maximum decomposition rate was achieved during the test was identified as the temperature of maximum point in the derivative weight curve (%/°C). The residue (usually carbonaceous material that cannot be further decomposed) was evaluated as remaining mass in percentage at the highest achieved temperature of TGA analysis (700 °C).

2.3.2. Differential Scanning Calorimetry (DSC)

Differential calorimetric tests were developed in a Q20 DSC, produced by TA Instruments (New Castle, DE, USA). A small piece of sample (8–10 mg) was subjected to the following thermal cycle under nitrogen atmosphere: (i) heating (first run) at 10 °C/min from 30 °C to 300 °C in order to delete the thermal history of the material, (ii) cooling (second run) at a constant rate of 10 °C/min up to 0 °C, (iii) reheating (3rd run) at the same rate up to 300 °C. The primary outcome of such experiments was the heat flow rate (mW) as a function of temperature (°C). From these data, the glass transition temperature (T_g), the melting temperature (T_m), the enthalpy of fusion (ΔH_f), and degree of crystallinity (x_c) were determined for each specific heating scan. The crystallization temperature (T_c) and the enthalpy of crystallization (ΔH_c) were calculated for the cooling scan. The glass transition (T_g) was identified as the temperature corresponding to the inflection point in the DSC signal. The melting and crystallization temperatures were recognized as temperatures corresponding to endothermic and exothermic peaks, respectively. The degree of crystallinity (x_c) was then calculated according to:

$$x_c = \frac{\Delta H_f}{\Delta H_f^0(1 - \emptyset)} \quad (1)$$

where \emptyset is the weight fraction of fibers in the composites, and ΔH_f^0 is the theoretical enthalpy of fusion for 100% crystalline PA 66 polymer (=197 J/g [31]).

2.3.3. Capillary Rheology

Capillary rheological tests were performed in a CEAST SmartRheo capillary rheometer, produced by Instron ITW Test and Measurement Italia S.r.l. (Turin, Italy) at 270 °C in the shear rate range from 100 to 10,000 s⁻¹. A capillary die, 1 mm in diameter and 30 mm in length, was adopted. The flow curves of the melted compounds were evaluated by neglecting the Bagley correction for the entrance pressure drop. The Mooney Rabinowitsch correction was applied to consider the non-Newtonian behavior of investigated materials, and non-parabolic velocity. This correction allowed the conversion of the measurements of pressure drop against the volume flow rate in the true wall shear rate and viscosity.

2.3.4. Scanning Electron Microscopy (SEM)

Samples were prepared by compression molding the pellets in a hydraulic press (mod. LP420B, produced by LabTech Engineering Company Ltd., Samut Prakarn, Thailand) under a pressure of 70 bar and a temperature of 270 °C. Then, samples were immersed in liquid

nitrogen and then broken. The brittle fracture surfaces were metallized through gold sputter coating. Morphological features of composites were highlighted using a field emission scanning electron microscope (SEM, Mod. TM 3000 Hitachi, Tokyo, Japan) operating at high vacuum conditions on the obtained metallized samples.

3. Results

3.1. Thermal Stability and Kinetic Parameters

TGA and DTGA curves of pure and filled PA 66 with glass and basalt fibers were presented in Figure 1.

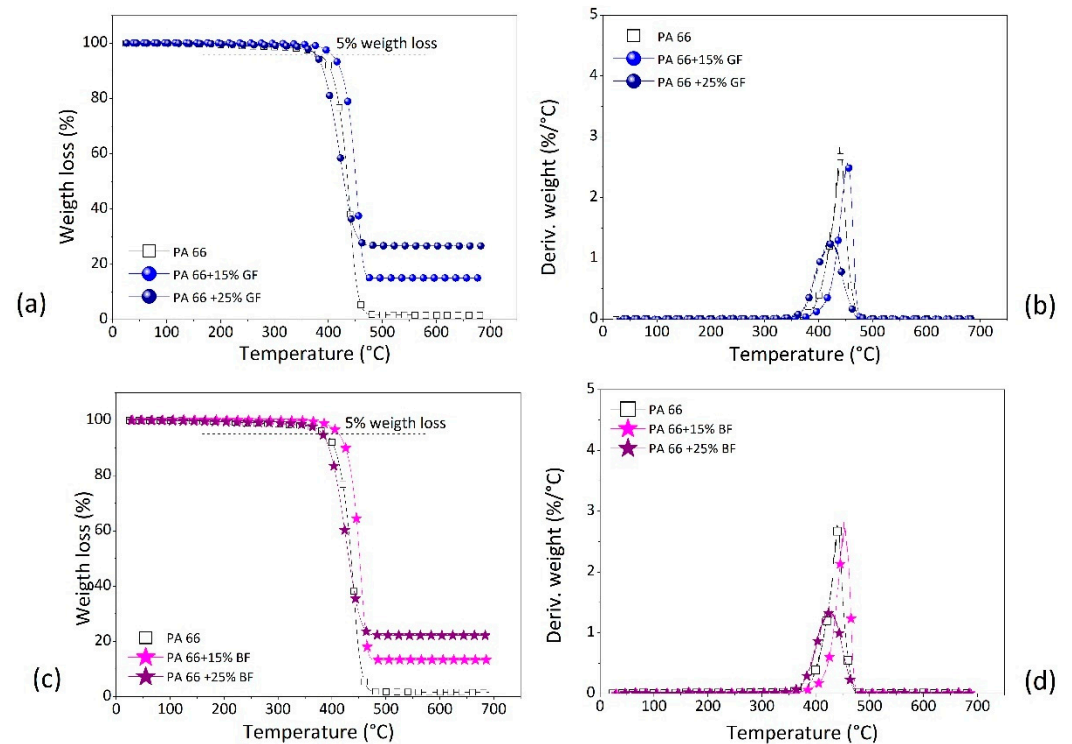


Figure 1. TGA thermograms of (a) GF/PA66 and (c) BF/PA66 composites, and DTGA of (b) GF/PA66 and (d) BF/PA66 composites.

At a heating rate of 20 °C/min, the TGA curve of pure PA 66 (black square points) showed one step of thermal degradation as a result of random chain scission process. The main organic products were eliminated in the form of hydrocarbons, nitriles and vinyl groups [32]. The thermal decomposition of polyamide 66 is a complex process involving hydrolysis, decarboxylation, deamination and dehydration, with release of water (H₂O), ammonia (NH₃), carbon dioxide (CO₂), cyclopentanone, adipic acid, hexadamine, nitrile and olefin [32].

A similar trend of the mass loss (%) curve against temperature was found in the case of composite systems. Regardless of filler type, for composites including a fiber concentration equal to 15 wt.%, the initial decomposition temperature (~410 °C) became higher with respect to neat PA 66 (390 °C), whereas when the filler concentration rose to 25 wt.% the initial decomposition temperature was decreased to about 380 °C. Then, by comparing compounds at an equal fiber content, the initial decomposition temperature was usually higher, even if only by a few degrees (°C), in composites containing basalt fibers against systems containing glass fibers.

These results were also analogously verified by the derivative weight curves (DTGA). The maximum degradation temperature of neat matrix (~441 °C) was shifted to higher values (~454 °C) when the fiber content was equal to 15 wt.% and was moved to smaller values (~425 °C) when the basalt fiber in the matrix amounted to 25 wt.%.

Usually, when fillers have been introduced to a matrix, an increased thermal stability has been verified. This outcome was attributed to the formation of tortuous pathways that slowed down the mass diffusion of the degradation products from the bulk of the polymer to the gas phase. In this case, the fibers acted as a protective barrier against the polymeric thermal decomposition. However, this finding was found to be dependent on filler type and its content. If on one side, when the filler loading was low, a barrier effect could be provoked that led to an improvement in the thermal stability; on the other side, at high filler loading, a promoter effect could be induced that encouraged the degradation process [33].

From the experimental data, it appeared that, at a content of 15% in wt., the fibers dispersed in the matrix exerted a barrier effect that hindered the polymer matrix decomposition. Then, if the fiber concentration was 25 wt.%, the barrier effect was overcome by the promoter effect, and it was determined to be an initial point for decomposition at lower temperatures with respect to the basic PA 66.

The final residue of PA 66 degradation was evaluated around 1.6% (remaining mass in correspondence of 700 °C). This value increased in composite systems in a proportional way to the introduced nominal filler content in PA 66 polymer during compounding. An appreciable agreement between the effective and the nominal filler content was confirmed.

TGA results were summarized in Table 1 for all the investigated materials.

Table 1. Initial decomposition temperature ($T_{dec5\%}$), temperature of the maximum rate of decomposition (T_{max}), and residue at 700 °C for the PA 66-based compounds.

	$T_{dec5\%}$	T_{max}	Residue at 700 °C
PA 66	390 °C	441 °C	1.58%
PA 66 + 15% GF	410 °C	454 °C	15.04%
PA 66 + 25% GF	380 °C	424 °C	26.69%
PA 66 + 15% BF	413 °C	454 °C	13.33%
PA 66 + 25% BF	383 °C	426 °C	22.16%

The rearranging of TGA data, in terms of weight loss (%) vs temperature (°C), has also made possible the evaluation of kinetic parameters of thermal decomposition for each type of material.

The conversional fraction (α), shown in Figure 2, was evaluated according to the Equation (2):

$$\alpha = \frac{m_0 - m}{m_0 - m_f} \quad (2)$$

where m_0 is the initial sample weight, m is the instantaneous sample weight at certain time t , m_f is the final sample weight.

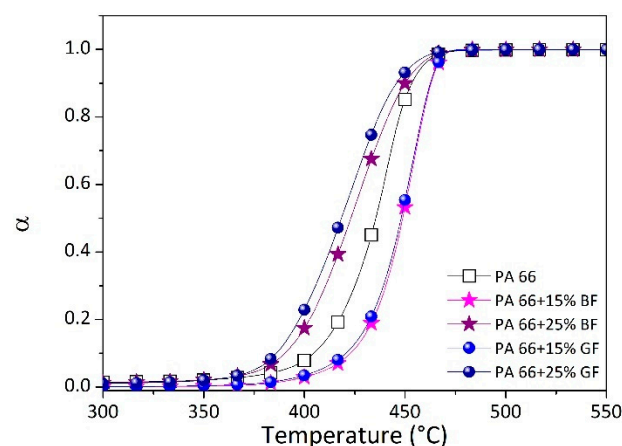


Figure 2. Conversional factor vs temperature for all investigated materials.

The conversion factor of PA 66 remained superior to composites incorporating 15 wt.% of filler loading, but inferior compared to composites at 25 wt.% of filler loading. At an equal fiber percentage, the α curve relating to compounds incorporating basalt fibers was almost coincident with that measured for compounds containing glass fibers.

The kinetics of the degradation reaction were performed by the isothermal rate of conversion $\left(\frac{d\alpha}{dt}\right)$ and the following equation (Equation (3)):

$$\frac{d\alpha}{dt} = K(T)f(\alpha) \quad (3)$$

where $K(T)$ is the constant of decomposition rate and $f(\alpha)$ is the reaction mechanism function for describing the kinetic thermal degradation [34].

$K(T)$ is described by the Arrhenius equation (Equation (4)):

$$K(T) = A \exp\left(-\frac{E_a}{RT}\right) \quad (4)$$

where A is the pre-exponential factor, E_a is the activation energy, and R is the universal gas constant ($8.314 \text{ J mol}^{-1} \text{ K}^{-1}$), T is the temperature in K.

Thus:

$$\frac{d\alpha}{dt} = A \exp\left(-\frac{E_a}{RT}\right) f(\alpha) \quad (5)$$

For a heating rate $\beta \left(= \frac{dT}{dt}\right)$, the Equation (5) can be written in an integral version (Equation (6)):

$$G(\alpha) = \int_0^\alpha \frac{d\alpha}{f(\alpha)} = \frac{A}{\beta} \int_{T_0}^{T_f} \exp\left(-\frac{E_a}{RT}\right) dT \quad (6)$$

$f(\alpha)$ or $g(\alpha)$, defined through several reaction models, were listed in [35].

Here, it has been considered:

$$f(\alpha) = (1 - \alpha) \quad (7)$$

$$G(\alpha) = (-\ln(1 - \alpha))^n \quad (8)$$

where n is the order of reaction.

The activation energy (E_a) has been calculated through the so-called Coats–Redfern method from a plot of $\ln[G(\alpha)/T^2]$ versus $1/T$, at a given conversion, and an order of reaction equal to 1.

The slope of the straight line fitting the experimental data was equal to $-E_a/R$, and the corresponding intercept was equal to $\ln\left(\frac{AR}{\beta E_a}\right)$ [36].

Figure 3 displayed a comparison among the $\ln[G(\alpha)/T^2]$ versus $1/T$ curves for all the materials.

The almost linear trend of $\ln[G(\alpha)/T^2]$ versus $1/T$ curves with high correlation coefficient (the lowest $R^2 = 0.968$ for PA6,6) confirmed that a correct model has been used for describing the reaction [35]. The kinetic parameters, i.e., the activation energy (E_a) and pre-exponential factor (A), were extracted from the Figure 3 and reported in Table 2.

Activation energy represents a barrier to be overcome to give life to a chemical reaction. The higher the activation energy, the more difficult it is for the reaction to occur [36].

The values of E_a were mostly affected by filler content more than filler type. No strong effect of filler type on activation energy of PA 66 was fully demonstrated. The compounds at 25 wt.% of fiber content possessed an activation energy comparable to neat matrix ($\sim 170 \text{ kJ/mol}$) that was inferior with respect to composites at 15 wt.% of fiber concentration ($\sim 230 \text{ kJ/mol}$). In terms of activation energy, a higher value was found in the case of composites incorporating basalt fibers with respect to those incorporating glass fibers, especially when the fiber content was around 15 wt.%.

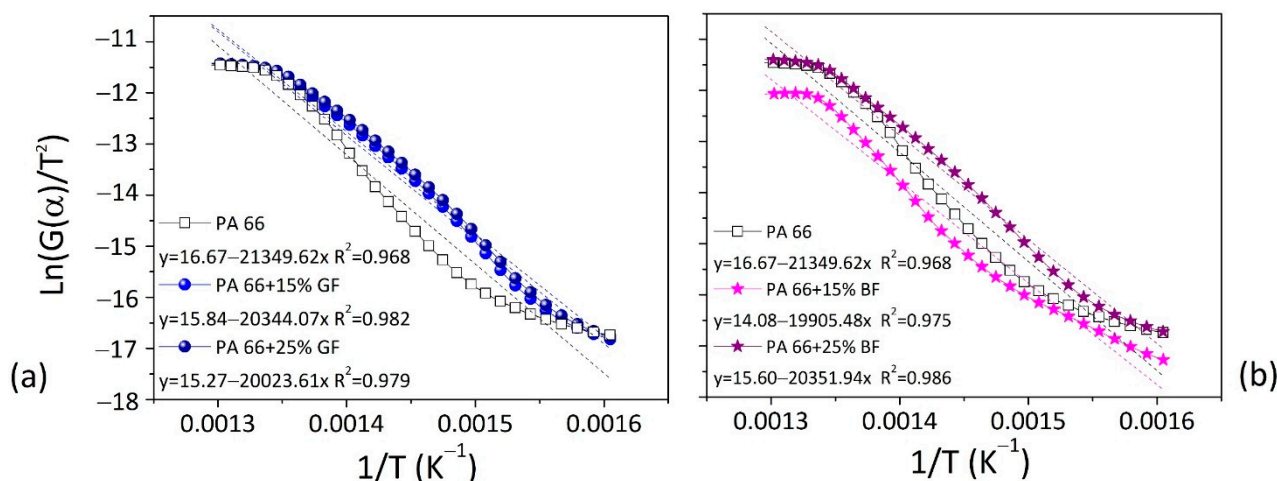


Figure 3. The Coats–Redfern method for PA 66 + GF composites (a) and PA 66 + BF composites (b).

Table 2. Kinetic parameters using CR method.

	E_a (kJ mol ⁻¹)	A (min ⁻¹)
PA 66	177	7.41×10^{12}
PA 66 + 15% GF	227	2.92×10^{16}
PA 66 + 25% GF	166	1.72×10^{12}
PA 66 + 15% BF	241	2.30×10^{17}
PA 66 + 25% BF	169	2.42×10^{12}

E_a here evaluated for neat PA 66 was slightly higher, but comparable, with the values reported in literature of 80–114 kJ/mol [32,37,38] (in all cases heating rate was 10 °C/min). Azimi and Abedifard found an activation energy of 200 kJ/mol, for PA 66 composites containing 10 wt.% of GF [38].

3.2. Glass Transition, Melt and Crystallization

The DSC thermograms of reinforced PA 66 based composites for heating and cooling treatments are presented in Figure 4.

First of all, it should be noted that, the properties found during the first heating scan were quite different to those found in the second heating scan for all the investigated materials, particularly for the composite systems. This was intended as a strong influence of the manufacturing process on the thermal characteristics of the compounds. In detail, the addition of both GF and BF in PA 66 matrix led to an increase in the melting temperature. During the first heating (Figure 4a,b), the melting peak started from a value of 245 °C for neat PA 66 and achieved a value around 256 °C for composites, regardless of filler content and type. The increment of melting temperature in composites both containing glass and basalt fiber, was confirmed also during the second heating (Figure 4e,f). In this case, the presence of two melting peaks were detected at 245 °C (T_{m1}) and 251 °C (T_{m2}) for GF/PA6,6 and BF/PA6,6 composites. The double endothermic peak in the heat flow curve was attributed to the existence of two crystalline structures: the α -crystalline portion and thermodynamically unstable γ -crystalline portion [39].

The crystallization temperature of GF/PA 66 and BF/PA 66 compounds was shifted towards higher temperatures compared to the neat resin. However, the incorporation of glass and basalt fibers into PA 66 matrix also resulted in a decrement in the degree of crystallinity (x_c), evident both in the first and second heating scan (Table 3).

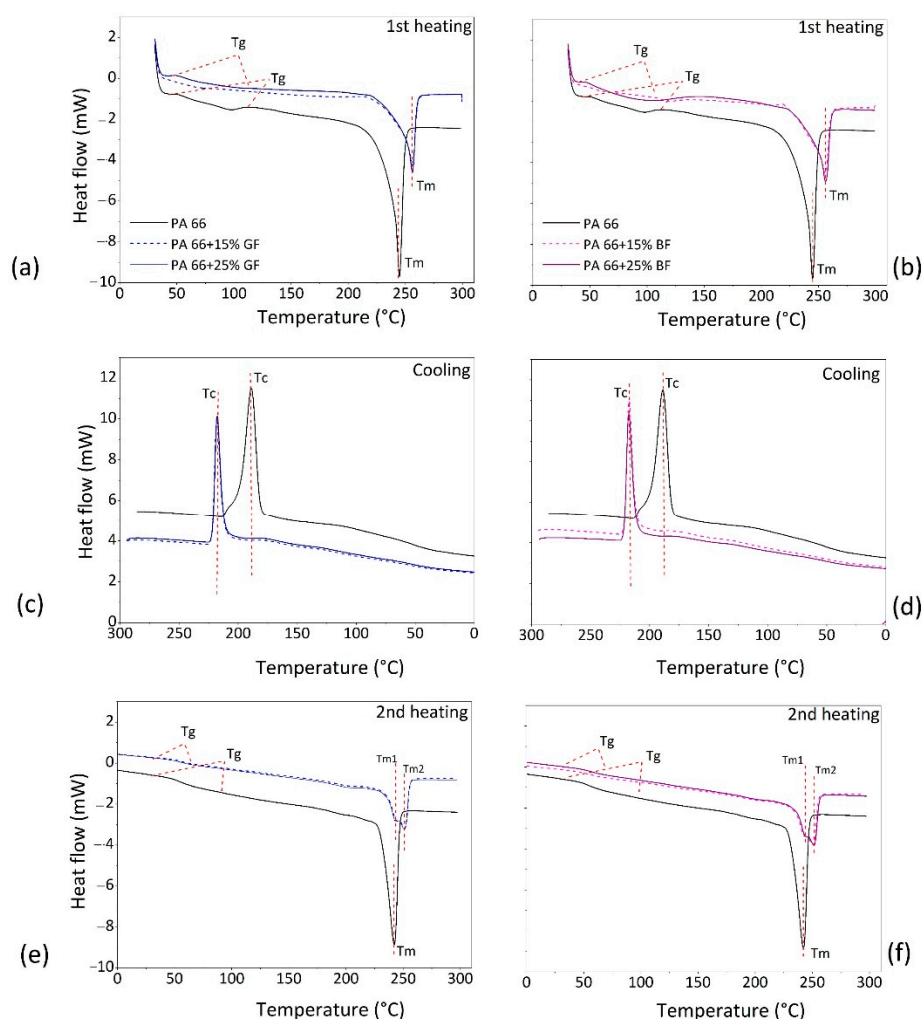


Figure 4. Heat flow curves as a function of temperature recorded during DSC thermal cycles for developed composites (legend in (c,e) as in (a), legend in (d,f) as in (b)).

If on one side, the fibers could act as a nucleating agent by promoting the nucleation of the matrix and increasing the crystallization temperature; then on the other side, when the content was elevated, they could limit the expansion of spherulites by reducing the crystallinity degree [40]. The reduction in the degree of crystallinity in composites compared to neat matrix, approximately amounted to 30% in the second heating scan, was intended as a strong change in the microstructure of the neat polymer (PA 66) when the fibers have been added. The presence of fibers inhibited the crystallization process, and hence, led to a reduction in the crystallinity degree [41].

By taking into account the second heating scan, the glass transition temperatures of composites were always comparable among themselves, and about 8 °C lower (~56 °C) than that recorded for the neat matrix (64 °C). Thus, both the glass and basalt fibers added to the PA6,6 have caused an increased chain mobility and lowered the activation energy barrier for segmental relaxations of the surrounding polymer molecules. This effect was attributed to a change in the local segmental package of polymer chains that led to an increase in free volume, and consequently, to the macromolecules mobility [42].

Finally, it could be concluded that, even if the fiber introduction into PA 66 has strongly affected the melting point, the crystallization and glass transition of the neat polymer, no effect of filler type and content could be highlighted on the thermal characteristics of BF/PA66 and GF/PA66 composites performed through DSC.

The calorimetric results in terms of melting (T_m) and crystallization (T_c) temperatures, melting (ΔH_f) and crystallization (ΔH_c) enthalpies, and the degree of crystallinity (x_c) are reported in Table 3 for all investigated materials.

Table 3. Thermal properties of the composite materials as obtained by DSC measurements.

1st Heating scan					
	T_g (°C)	T_m (°C)		ΔH_f (J/g)	x_c
PA 66	62	245		54.26	0.28
PA 66 + 15% GF	n.d.	256		41.69	0.25
PA 66 + 25% GF	62	256		36.21	0.25
PA 66 + 15% BF	n.d.	256		37.63	0.22
PA 66 + 25% BF	62	256		32.09	0.22
Cooling					
	T_c (°C)			ΔH_c (J/g)	
PA 66	189			48.41	
PA 66 + 15% GF	218			31.37	
PA 66 + 25% GF	218			25.10	
PA 66 + 15% BF	217			27.55	
PA 66 + 25% BF	218			25.76	
2nd Heating scan					
	T_g (°C)	T_{m1} (°C)	T_{m2} (°C)	ΔH_f (J/g)	x_c
PA 66	64	243	/	48.54	0.25
PA 66 + 15% GF	56	245	251	40.96	0.24
PA 66 + 25% GF	56	245	252	33.81	0.23
PA 66 + 15% BF	55	245	251	35.3	0.21
PA 66 + 25% BF	56	245	252	29.87	0.20

3.3. Shear Viscosity

The processing and shaping of materials are aspects strictly related to their ability to be deformed and to their flow resistance. On this basis, the analysis of rheological properties, developed in a capillary circular die, at temperatures higher than the material melting, and at the typical shear rates encountered in extrusion and injection molding technologies (10^2 – 10^4 s⁻¹), was a practice extremely useful to gain information on the processing behavior of the developed compounds.

The shear viscosity (Pa*s) as a function of the shear rate (s⁻¹), measured at temperature equal to 270 °C, is displayed in Figure 5 for GF/PA66 and BF/PA66 composites, and the neat polyamide resin.

Usually, the trend of viscosity vs shear rate for neat polymer can be divided into two regions. The first is characterized by a horizontal stoke, during which the viscosity remained at a constant value, also identified as the Newtonian region. The second is described by a decreasing trend of viscosity as the shear rate was increased, also identified as shear-thinning region or pseudo-plastic behavior. From the data, the viscosity trend of neat PA 66 showed a slightly perceptible Newtonian plateau around a value of 10² Pa*s. After a shear rate of 10³ s⁻¹, a shear-thinning trend was followed with decreasing viscosity as the shear rate increased. The flow behavior of neat matrix was fully changed by the introduction of both BF and GF fibers. In fact, in the composites, the Newtonian region was lost and the shear thinning behavior persisted throughout the entire shear rate. The viscosity increase was affected both by filler content and type. At 15 wt.% GF fibers, and

higher shear rates ($>5 \times 10^2 \text{ s}^{-1}$) the viscosity values were very similar to the PA 66 matrix and detached from those of the neat resin as the shear rate decreased. At 25 wt.% GF content, the shear viscosity was found to be over the values found for composites at 15 wt.% of GF loadings, but slightly lower compared to composites at 15 wt.% BF fibers. Finally, at 25 wt.% BF content, the highest increase in melt viscosity was recorded compared to all the other investigated systems.

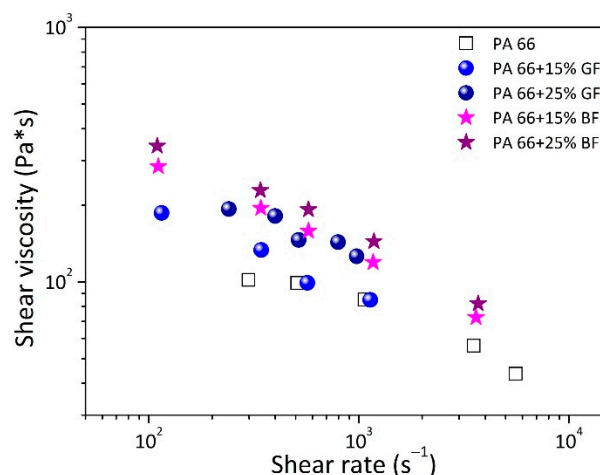


Figure 5. Real viscosity vs. shear rate evaluated at 270 °C for filled and neat PA 66.

It can be supposed that the introduction of fibers in PA 66 led to a constraint in the macromolecular chains' motion that increased the viscosity of the melted systems compared to the basic polymer, particularly at low shear rate. It was demonstrated that at low shear rates, the fibers were moved and rotated with respect to the flow path, assuming a random position. This led to a greater possibility of fiber-to-fiber collision which resulted in an increased flow resistance, also as the fiber content was increased. At high shear rate the material moved almost like a plug, the fibers became oriented in the flow direction, the fiber–fiber collision was much less possible, and the viscosity increase, due to the increase in content of fibers present, was lower [43]. Furthermore, two other factors could contribute to the mild increase in viscosity of composites compared to the matrix at high shear rates: the first was the possible breakdown of the fibers at the capillary inlet, which were thus more easily dispersed and oriented in the flow direction; the second was the weak interaction between fiber and matrix due to poor compatibility between the two phases [33].

The simplest model that can be used to capture such behavior is the power-law, or Ostwald-de Waele model [44]:

$$\eta(\dot{\gamma}) = \kappa \dot{\gamma}^{n-1} \quad (9)$$

where $\dot{\gamma}$ is the shear rate, κ is the consistency ($\text{Pa}\cdot\text{s}^n$) and n is the flow index. Shear thinning behavior is represented by $n < 1$; shear-thickening behavior is symbolized by $n > 1$; Newtonian behavior is associated to $n = 1$. For n in the range between 0 and 1, the smaller the n value, the greater the degree of shear-thinning and the sensitivity of polymer to the shear rate changes (beneficial for the processing).

The experimental data reported in Figure 5 was fitted according to the power law equation (Equation (9)). The consistency and flow index were evaluated, and reported in Figure 6, both for matrix and corresponding GF/PA66 and BF/PA66 composites. The coefficients of determination (R^2) resulted to be superior to 0.98 for any regression.

It can be observed that consistency strongly increased with the filler content, and particularly in the case of basalt fibers. For BF/PA 66 composites at 25 wt.% of loading, the consistency grew by four-fold with respect to the value evaluated for basic PA 66. On the contrary, the flow index showed a very weak dependency on the filler concentration, particularly in the case of glass fibers. Actually, the value was equal to 0.7 for the neat polymer and oscillated around 0.6 in the case of composites. In other words, the shear

thinning degree of composites at 15 and 25 wt.% GF concentrations, was very similar to the matrix, whereas in the case of composites containing BF, the shear thinning attitude seemed to slightly increase by increasing the fiber loadings. In this latter case, the higher degree of shear thinning was explained with an increase in local shear rate induced in the thin polymer layer in the space between the BF fibers [45].

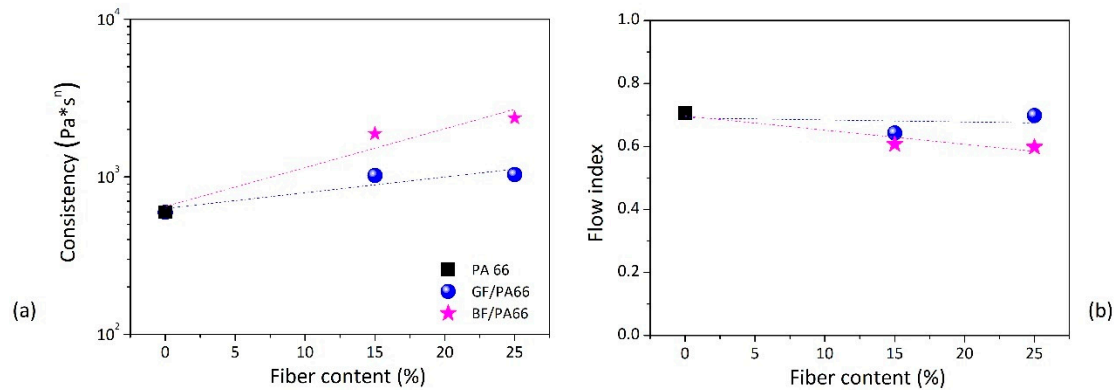


Figure 6. Consistency (a) and index flow (b) against filler loading. Lines in figures are to guide the eyes.

3.4. Morphological Aspects

SEM images of GF/PA 66 compounds are reported in Figure 7a,b at 15 and 25 wt.% in fiber content, respectively. BF/PA66 is shown in Figure 7d,e, at 15 and 25 wt.%, in fiber content, respectively.

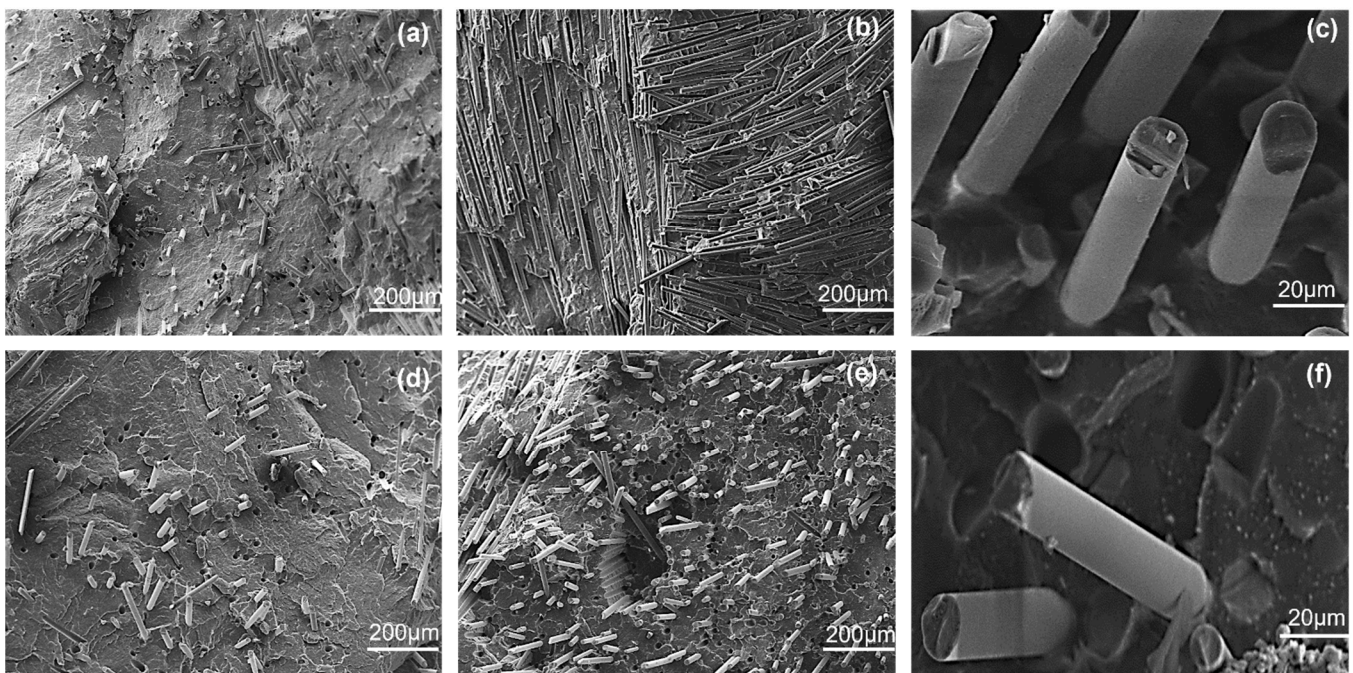


Figure 7. SEM micrographs of PA 66 compounds reinforced with 15 wt.% (a) and 25 wt.% (b) of GF; or 15 (d) and 25 wt.% (e) of BF at scale bar of 200 μm. SEM micrographs of PA66/GF (c) and PA66/BF (f) at scale bar of 20 μm.

In both systems, a random orientation of fibers throughout the matrix was observed. At 15 wt.% of filler loading, the fibers appeared well isolated from each other in the polymer resin, without evident signs of agglomeration. There were different considerations in the case of composites at 25 wt.% of fiber. In detail, in the GF/PA66 composites, undispersed fiber bundles could be observed. In the case of BF/PA66 composites, the fibers seemed

to be more than double those contained in the sample at loading equal to 15 wt.%. These last observations attested to a worsening of fiber dispersion when the related content was increased in the matrix.

However, the presence of cavities and holes on the samples' surface was considered a direct consequence of pull out and debonding phenomena occurring during the preparation of cryogenic fracture surfaces. These phenomena were usually verified in the field of reinforced polymer matrices. Under load conditions, at a certain point the matrix began to yield. The fiber continued to sustain the load up to a limit that corresponded to the failure strength of filler/matrix interface (debonding). Beyond this limit, the fiber was deformed until it slipped out, leaving a vacuum in the matrix (pull-out) [33].

The extracted fibers showed no signs of polymer wrapping and surface covered by polyamide (Figure 7c,f). This indicated that the fibers and matrix were not well combined, and weak interfacial adhesion between the two phases was achieved both in the case of GF and BF compounds.

4. Conclusions

In this work, the performance of BF/PA66 and GF/PA66 composites (at fiber contents of 15 and 25 wt.%) have been compared in terms of thermal stability, glass transition, crystallization and melting point, shear viscosity, and morphological aspects.

Depending upon the content, the presence of added fibers (both BF and GF) to PA 66 matrix could speed up or slow down the polymer decomposition by heat. PA66 matrix possessed a thermal stability lower than composites at 15 wt.% of fiber loading, and higher than systems incorporating 25 wt.% fiber content. The initial decomposition temperature and evaluated activation energy for thermal degradation, were found to be higher in the case of composites incorporating basalt fibers, particularly at 15 wt.% in content, albeit mildly.

The crystallization temperature of BF/PA66 and GF/PA66 systems was determined to be around 218 °C, that was about 30 °C higher with respect to the value of basic PA66. On the contrary, the degree of crystallinity was decreased approximately 20% when the fibers were incorporated into the neat polymer. The presence of fibers, acting as nucleating agents, promoted the crystallization during the cooling phase of the polymeric melt, but the formation of crystalline structures was limited by the large dimensions of the fibers themselves (reducing the crystallinity degree). As concerning the melting point, the existence of a double endothermic peak at 245 °C and 251 °C for the BF/PA66 and GF/PA66 systems, instead of a single endothermic peak at 243 °C displayed for the neat matrix, was attributed to the formation of two crystalline arrangements, one stable and another thermodynamically unstable. A similar glass transition temperature (equal to 56 °C) was verified for all the composites, however they were approximately 7–8 °C lower than the neat matrix (~64 °C).

The melt viscosity of the neat PA66 displayed a perceptible Newtonian plateau followed by a decreasing trend, increasing the shear rate. In the case of composites, the Newtonian plateau disappeared, and a shear thinning behavior was observed with viscosity values higher than the neat resin, particularly at low shear rate and in the BF/PA66 systems. Morphological aspects from SEM micrographs revealed debonding and pull-out phenomena of fibers from the matrix, leaving holes on the sample surface and bare pieces of fiber without polymer covering. These aspects were considered signs of poor compatibility between filler and matrix, both in the case of BF/PA66 and GF/PA66 composites.

Finally, it was concluded that the effect of basalt content introduced into the PA 66 matrix equal to 15 or 25 wt.% on investigated features was quite similar, and comparable to that caused by glass fiber incorporation, at the same amount, in the same matrix. A future study could aim to improve the compatibility and interfacial adhesion between the two phases by proposing appropriate formulations involving fiber sizing, coupling, and/or agents to enhance compatibility.

Author Contributions: Conceptualization, L.N.; validation, D.A., data curation, A.P. and L.G.; writing—original draft preparation, A.P.; writing—review and editing, S.A. and L.N.; supervision, D.A. All authors have read and agreed to the published version of the manuscript.

Funding: This research received no external funding.

Institutional Review Board Statement: Not applicable.

Informed Consent Statement: Not applicable.

Data Availability Statement: The data presented in this study are available on request from the corresponding author.

Acknowledgments: S. Acierno acknowledges the support of the Italian Ministry of University, project PRIN 2017, 20179SWLKA “Multiple Advanced Materials Manufactured by Additive technologies (MAMMA)”. A. Patti wishes to thank the Italian MIUR in the framework of Action 1.2 “Researcher Mobility” of The Axis I of PON R&I2014-2020 under the call “AIM—Attrazione e Mobilità Internazionale”.

Conflicts of Interest: The authors declare no conflict of interest.

References

1. Jain, N.; Verma, A.; Singh, V.K.; Li, Z.; Ma, J.; Ma, H.; Xu, X. Properties and Applications of Basalt Fiber and Its Composites. *IOP Conf. Ser. Earth Environ. Sci.* **2018**, *186*, 012052. [[CrossRef](#)]
2. Nakonieczny, D.S.; Antonowicz, M.; Paszenda, Z. Surface modification methods of ceramic filler in ceramic-carbon fibre composites for bioengineering applications—A systematic review. *Rev. Adv. Mater. Sci.* **2020**, *59*, 586–609. [[CrossRef](#)]
3. Manickam, R.; Pradeep, P.; Raja, J.E.; Ramachandran, D.M.; Stanly, B.; Retnam, J. Mechanical Characterization of jute fiber over glass and carbon fiber reinforced polymer composites. *Int. J. Appl. Eng. Res.* **2015**, *10*, 10392–10396.
4. Irawan, A.P.; Fitriyana, D.F.; Tezara, C.; Siregar, J.P.; Laksmidewi, D.; Baskara, G.D.; Abdullah, M.Z.; Junid, R.; Hadi, A.E.; Hamdan, M.H.M.; et al. Overview of the Important Factors Influencing the Performance of Eco-Friendly Brake Pads. *Polymers* **2022**, *14*, 1180. [[CrossRef](#)]
5. Jamshaid, H.; Mishra, R. A green material from rock: Basalt fiber—A review. *J. Text. Inst.* **2015**, *107*, 923–937. [[CrossRef](#)]
6. Ross, A. Basalt Fibers: Alternative to Glass? *Compos. Technol.* **2006**, *12*, 44–48.
7. Kogan, F.M.; Nikitina, O.V. Solubility of chrysotile asbestos and basalt fibers in relation to their fibrogenic and carcinogenic action. *Environ. Health Perspect.* **1994**, *102*, 205–206. [[CrossRef](#)]
8. Haldar, S.K.; Tišljarić, J. *Introduction to Mineralogy and Petrology*; Elsevier: Amsterdam, The Netherlands, 2013; pp. 1–338. [[CrossRef](#)]
9. Krayushkina, K.; Khymeryk, T.; Bieliatynskyi, A. Basalt fiber concrete as a new construction material for roads and airfields. *IOP Conf. Ser. Mater. Sci. Eng.* **2019**, *708*, 012088. [[CrossRef](#)]
10. Liu, J.; Chen, M.; Yang, J.; Wu, Z. Study on Mechanical Properties of Basalt Fibers Superior to E-glass Fibers. *J. Nat. Fibers* **2020**, *19*, 882–894. [[CrossRef](#)]
11. Patti, A.; Acierno, S.; Cicala, G.; Zarrelli, M.; Acierno, D. Recovery of Waste Material from Biobags: 3D Printing Process and Thermo-Mechanical Characteristics in Comparison to Virgin and Composite Matrices. *Polymers* **2022**, *14*, 1943. [[CrossRef](#)]
12. Patti, A.; Acierno, D. Towards the Sustainability of the Plastic Industry through Biopolymers: Properties and Potential Applications to the Textiles World. *Polymers* **2022**, *14*, 692. [[CrossRef](#)] [[PubMed](#)]
13. Balaji, K.V.; Shirvanimoghaddam, K.; Rajan, G.S.; Ellis, A.V.; Naebe, M. Surface treatment of Basalt fiber for use in automotive composites. *Mater. Today Chem.* **2020**, *17*, 100334. [[CrossRef](#)]
14. Bhat, T.; Fortomaris, D.; Kandare, E.; Mouritz, A.P. Properties of thermally recycled basalt fibres and basalt fibre composites. *J. Mater. Sci.* **2018**, *53*, 1933–1944. [[CrossRef](#)]
15. Jamshaid, H.; Mishra, R.; Militky, J.; Hussain, T. Analysis of Basalt and Thermoplastic Hybrid Composites. *J. Fiber Bioeng. Inform.* **2018**, *11*, 163–174. [[CrossRef](#)]
16. San, V.; Arnanz, M.; Fernández, J.P.; Liu, H.; Yu, Y.; Liu, Y.; Zhang, M.; Li, L.; Ma, L.; Sun, Y.; et al. A Review on Basalt Fiber Composites and Their Applications in Clean Energy Sector and Power Grids. *Polymers* **2022**, *14*, 2376. [[CrossRef](#)]
17. Liu, Q.; Shaw, M.T.; Parnas, R.S.; McDonnell, A.M. Investigation of Basalt Fiber composite mechanical properties for applications in Transportation. *Polym. Compos.* **2006**, *27*, 41–48. [[CrossRef](#)]
18. Monaldo, E.; Nerilli, F.; Vairo, G. Basalt-based fiber-reinforced materials and structural applications in civil engineering. *Compos. Struct.* **2019**, *214*, 246–263. [[CrossRef](#)]
19. Davies, P.; Verbouwe, W. Evaluation of Basalt Fibre Composites for Marine Applications. *Appl. Compos. Mater.* **2018**, *25*, 299–308. [[CrossRef](#)]
20. Nayak, S.Y.; Sultan, M.T.H.; Shenoy, S.B.; Kini, C.R.; Samant, R.; Shah, A.U.M.; Amuthakkannan, P. Potential of Natural Fibers in Composites for Ballistic Applications—A Review. *J. Nat. Fibers* **2020**, *19*, 1648–1658. [[CrossRef](#)]
21. Mishnaevsky, L.; Branner, K.; Petersen, H.N.; Beauson, J.; McGugan, M.; Sørensen, B.F. Materials for Wind Turbine Blades: An Overview. *Materials* **2017**, *10*, 1285. [[CrossRef](#)]

22. Kurańska, M.; Barczewski, M.; Uram, K.; Lewandowski, K.; Prociak, A.; Michałowski, S. Basalt waste management in the production of highly effective porous polyurethane composites for thermal insulating applications. *Polym. Test.* **2019**, *76*, 90–100. [[CrossRef](#)]
23. Osei Bonsu, A.; Liang, W.; Mensah, C.; Yang, B. Assessing the mechanical behavior of glass and basalt reinforced vinyl ester composite under artificial seawater environment. *Structures* **2022**, *38*, 961–978. [[CrossRef](#)]
24. Rajawat, A.S.; Singh, S.; Gangil, B.; Ranakoti, L.; Sharma, S.; Asyraf, M.R.M.; Razman, M.R. Effect of Marble Dust on the Mechanical, Morphological, and Wear Performance of Basalt Fibre-Reinforced Epoxy Composites for Structural Applications. *Polymers* **2022**, *14*, 1325. [[CrossRef](#)] [[PubMed](#)]
25. Zhang, C. Progress in semicrystalline heat-resistant polyamides. *E-Polymers* **2018**, *18*, 373–408. [[CrossRef](#)]
26. Liao, G.; Li, Z.; Luan, C.; Wang, Z.; Yao, X.; Fu, J. Additive Manufacturing of Polyamide 66: Effect of Process Parameters on Crystallinity and Mechanical Properties. *J. Mater. Eng. Perform.* **2022**, *31*, 191–200. [[CrossRef](#)]
27. Makhlof, A.; Layachi, A.; Kouadri, I.; Belaadi, A.; Satha, H. Structural study and thermal behavior of composites: Polyamide 66/glass fibers: The reinforcement ratio effect on the kinetics of crystallization. *J. Compos. Mater.* **2019**, *54*, 1467–1481. [[CrossRef](#)]
28. Kumar Kundu, C.; Li, Z.; Song, L.; Hu, Y. Flame Retardant Treatments of Nylon Textiles: A Shift towards Eco-Friendly Approaches. In *Flame Retardant and Thermally Insulating Polymers*; IntechOpen: London, UK, 2021. [[CrossRef](#)]
29. Charles, J.; Ramkumaar, G.R.; Azhagiri, S.; Gunasekaran, S. FTIR and thermal studies on nylon-66 and 30% glass fibre reinforced nylon-66. *E-J. Chem.* **2009**, *6*, 23–33. [[CrossRef](#)]
30. Lee, J.Y.; Kim, K.J. MEG Effects on Hydrolysis of Polyamide 66/Glass Fiber Composites and Mechanical Property Changes. *Molecules* **2019**, *24*, 755. [[CrossRef](#)]
31. Navarro-Pardo, F.; Martínez-Barrera, G.; Martínez-Hernández, A.L.; Castaño, V.M.; Rivera-Armenta, J.L.; Medellín-Rodríguez, F.; Velasco-Santos, C. Effects on the Thermo-Mechanical and Crystallinity Properties of Nylon 6,6 Electrospun Fibres Reinforced with One Dimensional (1D) and Two Dimensional (2D) Carbon. *Materials* **2013**, *6*, 3494–3513. [[CrossRef](#)]
32. Ribeiro, B.; Nohara, L.B.; Oishi, S.S.; Costa, M.L.; Botelho, E.C. Nonoxidative thermal degradation kinetic of polyamide 6,6 reinforced with carbon nanotubes. *J. Thermoplast. Compos. Mater.* **2012**, *26*, 1317–1331. [[CrossRef](#)]
33. Patti, A.; Nele, L.; Zarrelli, M.; Graziosi, L.; Acierno, D. A Comparative Analysis on the Processing Aspects of Basalt and Glass Fibers Reinforced Composites. *Fibers Polym.* **2021**, *22*, 1449–1459. [[CrossRef](#)]
34. Wan, H.; Huang, Z. Kinetic analysis of pyrolysis and thermo-oxidative decomposition of tennis string nylon wastes. *Materials* **2021**, *14*, 7564. [[CrossRef](#)] [[PubMed](#)]
35. Ebrahimi-Kahrizsangi, R.; Abbasi, M.H. Evaluation of reliability of Coats-Redfern method for kinetic analysis of non-isothermal TGA. *Trans. Nonferrous Met. Soc. China* **2008**, *18*, 217–221. [[CrossRef](#)]
36. Chen, C.; Bu, X.; Huang, D.; Huang, Y.; Huang, H. Thermal Decomposition and Kinetics Analysis of Microwave Pyrolysis of Dunaliella salina Using Composite Additives. *Bioenergy Res.* **2020**, *13*, 1205–1220. [[CrossRef](#)]
37. Herrera, M.; Matuschek, G.; Kettrup, A. Main products and kinetics of the thermal degradation of polyamides. *Chemosphere* **2001**, *42*, 601–607. [[CrossRef](#)]
38. Azimi, H.; Abedifard, P. Determination of activation energy during the thermal degradation of Polyamide 66/glass fiber composites. *J. Thermoplast. Compos. Mater.* **2020**, *33*, 956–966. [[CrossRef](#)]
39. Hassan, A.; Rahman, N.A.; Yahya, R. Moisture absorption effect on thermal, dynamic mechanical and mechanical properties of injection-molded short glass-fiber/polyamide 6,6 composites. *Fibers Polym.* **2012**, *13*, 899–906. [[CrossRef](#)]
40. Wang, Y.; Cheng, L.; Cui, X.; Guo, W. Crystallization Behavior and Properties of Glass Fiber Reinforced Polypropylene Composites. *Polymers* **2019**, *11*, 1198. [[CrossRef](#)]
41. Zhu, J.; Abeykoon, C.; Karim, N. Investigation into the effects of fillers in polymer processing. *Int. J. Lightweight Mater. Manuf.* **2021**, *4*, 370–382. [[CrossRef](#)]
42. Defelice, J.; Lipson, J.E.G. The influence of additives on polymer matrix mobility and the glass transition. *Soft Matter*. **2021**, *17*, 376–387. [[CrossRef](#)]
43. Crowson, R.J.; Folkes, M.J. Rheology of short glass fiber-reinforced thermoplastics and its application to injection molding. II. The effect of material parameters. *Polym. Eng. Sci.* **1980**, *20*, 934–940. [[CrossRef](#)]
44. Patti, A.; Cicala, G.; Acierno, S. Rotational Rheology of Wood Flour Composites Based on Recycled Polyethylene. *Polymers* **2021**, *13*, 2226. [[CrossRef](#)] [[PubMed](#)]
45. Carrino, L.; Ciliberto, S.; Giorleo, G.; Prisco, U. Effect of filler content and temperature on steady-state shear flow of wood/high density polyethylene composites. *Polym. Compos.* **2011**, *32*, 796–809. [[CrossRef](#)]